Proceedings World Geothermal Congress 2015
Melbourne, Australia, 19-25 April 2015

Petrophysical Anisotropies: Relation Between Properties and Influence in Peri-Volcanic Reservoir Modelling and Simulation

Gael Perry and Yves Géraud

GeoRessources Lab. – 2 rue du Doyen Marcel Roubault – 54518 Vandoeuvre-lès-Nancy – France

gael.perry@univ-lorraine.fr – yves.geraud@univ-lorraine.fr

Keywords: Bouillante, petrophysics, modelling, anisotropies, Tough2, flow simulation, reservoir, heritage

ABSTRACT

Peri-volcanic reservoirs, in geothermal context, can be a high-enthalpy source of energy, and be a solution to grow energy independence in some countries. Reservoir modelling permits to obtain information about fluid circulations and to validate a theoretical geometry. This geometry is controlled by the repartition of fracture network and the petrophysical properties of the rock.

In many models, petrophysical properties are considered isotropic. In real reservoir, the architecture is heterogeneous due to deposition process (lava flows, volcano-sedimentary flows, ash deposit, etc.) We establish three anisotropic preferential directions in some volcanic and volcano-sedimentary samples in thermal conductivity, speeds of P-wave propagation and permeability.

We create a simple theoretical model based on real dataset from Bouillante geothermal field (Guadeloupe, Lesser Antilles), and integrate petrophysical measured properties. We finally observe the influence of petrophysical anisotropies integrated the model in Tough2 software in order to simulate thermal and fluid transfers in the reservoir. Those simulations highlight the importance of anisotropies in horizontal transfers.

1. INTRODUCTION

Most of arc island volcanoes are very active and many little islands are created by those volcanic activities, for example in the Lesser Antilles. In this context, geothermal activity can be important and a guarantee in the way of energetic independence. The aim of this study is to better understand peri-volcanic geothermal reservoirs, based on laboratory measurements and numerical modelling.

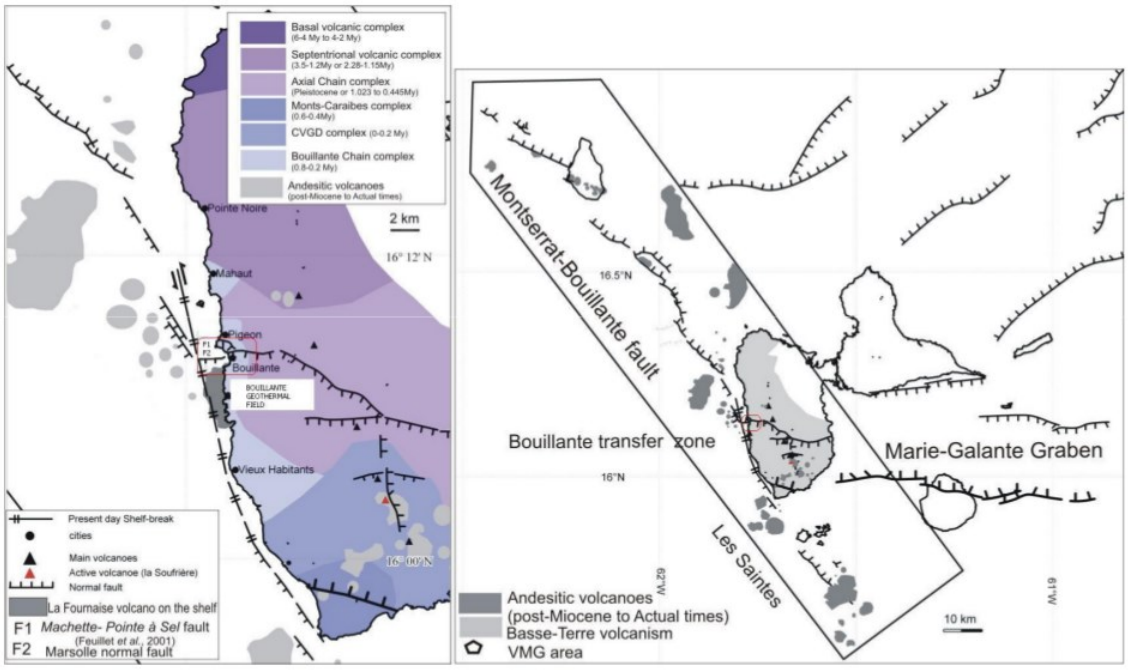

Figure 1: Regional context and structural map of the Bouillante geothermal field, from Bouchot et al. (2010).

Many models about geothermal reservoirs in the Lesser Antilles are high-scale models, e.g. Lachassagne et al. (2009), Bouchot et al. (2010), Lopez et al. (2010), for Guadeloupe example. They are mainly based on high-scale faults analysis, considering these faults as preferential circulation ways in water vertical movements. Calcagno et al. (2012) realised a structural 3D-model describing relations between different fault families and the implication of regional-scale structures. It appears that Marie-Galante Graben and Montserrat-Bouillante fault seem to drive main fault orientations at the geothermal scale of Bouillante groundwater reservoir (cf. Figure 1). Some geochemical studies have been made on geothermal fluids (at surface and in bore holes) in order to obtain dimensions of the Bouillante field, and composition of the groundwater, e.g. Mas et al. (2006), Bouchot et al. (2010), Bourdon et al.

(2011). These structural models are only based on geometrical features to determine circulation ways. Petrophysical studies exist in Lesser Antilles, e.g. Bernard et al. (2007) for example, but are mainly disconnected from modelling. The aim here will be to connect both studies, although we will be the most realistic in entries parameters during modelling.

Models considering realistic petrophysical properties are often built with isotropic datasets. In natural cases (which are a hundred per cent of our studies), rock formations are anisotropic. These petrophysical anisotropies (in thermal conductivity, wave propagation speed, permeability) have a great influence on reservoir comportment. On one hand, bedrock heritage, deposit processes, post-deposit deformations can create anisotropies, and the history of the field gives us some clues about them. On the other hand, petrophysical study of eventual anisotropies could provide us much information about geological history. Our method proposes to characterise properties on volcanic samples along three study planes and extrapolate data in order to build a 3D-ellipsoid representing anisotropy.

This petrophysical study will give us information about anisotropies in typical volcanic rocks. Based on past work on Bouillante geothermal field, we propose to compare models in order to understand the influence of petrophysical anisotropies in flowing simulation. These models can give a good estimation of thermal evolution of a peri-volcanic reservoir, to better manage geothermal field sustainability. Moreover, these flowing simulations will highlight the importance of horizontal and matrix circulation inside a modelling block.

2. PETROPHYSICS

The first step of this study is to determine petrophysical anisotropies. To characterize our samples, we worked on different methods, before comparing results and using them in modelling.

2.1 Laboratory Methods

Samples have been measured by four laboratory methods. First, we measured P-wave propagation speed, using Pundit Lab instrument. It can give us information about mineral composition and organisation, porosity network and micro-fracturing presence, e.g. Birch (1960). Then, we measured thermal conductivity, using Thermal Conductivity Scanner (TCS), which is based on the optical scanning method, e.g. Popov et al. (1999). Information gave by this second method are additional to the propagation speed. Third, we used Anisotropy of Magnetic Susceptibility (AMS) measurements in order to try to discriminate preferential magnetic petrofabric, e.g. Nédélec and Bouchez (2011). These results are not described here because of the weak anisotropy of our samples. Finally, we measured permeability on another sample, using TinyPerm-II field permeameter.

Samples are selected from volcanic formations in France and Germany (Nideck and Kaiserstuhl). We chose to study these samples because of the varieties of their compositions. From the Nideck, we studied two rhyolite samples from two different flows. Formation process is already discussed between lava and ignimbrite flow, e.g. Saucier et al. (1959), and we will speak here about rhyolite. These samples are named NI13-01 and NI13-02. From the Kaiserstuhl (cf. Figure 2), we first studied a sample from a lava flow (KA13-14), with same methods than Nideck's. Then, we chose a second sample (KA13-10) from volcano-sedimentary deposit. This sample was selected because it presented a macroscopic anisotropy (probably deposit surfaces), and in order to make some permeability measurements on it.

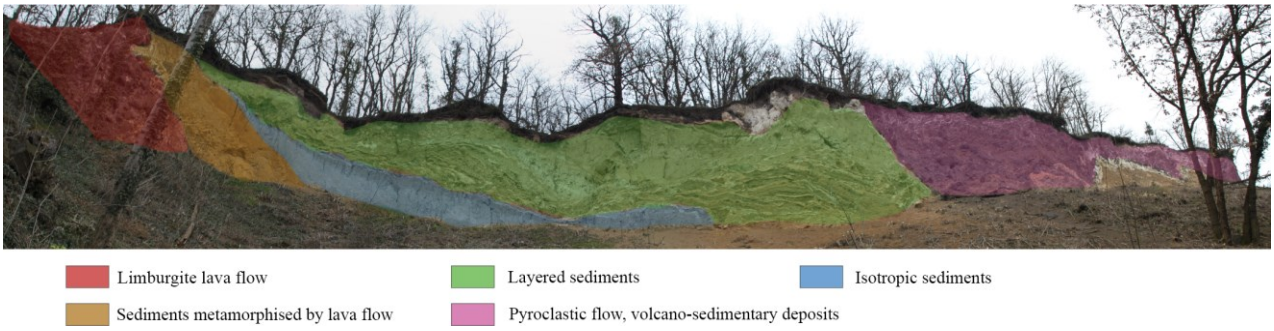

Figure 2: Volcano-sedimentary sequence from a Kaiserstuhl outcrop. Localisation of sample KA13-10 is situated in the pyroclastic flow and KA13-14 is in limburgite lava flow.

For samples NI13-01, NI13-02 and KA13-14, we created plugs in three orthogonal directions A, B and C. Then, we measured P-wave propagation and thermal conductivity in radial direction, every 10°. That operation permits to obtain values along three orthogonal plans, in order to approximate 3D anisotropies. In order to compare anisotropy values and directions, we created 3D-ellipsoid through least squares method. Then, we extracted anisotropy percentage, the type of ellipsoid (oblate-prolate) and the relation between P-wave propagation speed and thermal conductivity anisotropies. For sample KA13-10, which is a volcano-sedimentary sample, we simply made a block, following apparent layering, and measured in the three directions P-wave propagation speed, thermal conductivity, and permeability. The results can provide us information to further inject in the numerical model.

After least squares method, we can extract two principles parameters to determine importance of petrophysical anisotropies. These two parameters provide us a good idea of ellipsoids characterization. We define anisotropy percentage:

$$P\% = 100 * \left(\frac{a}{c} - 1\right)$$

where *P*% is the anisotropy percentage, *a* is the taller axe and *c* the smaller axe of the ellipsoid. To examine the shape of the ellipsoid, we define Jelinek shape parameter:

$$T = \frac{\log F - \log L}{\log F + \log L}$$

where *T* is the Jelinek parameter, *F* the planar anisotropy and *L* the linear anisotropy:

$$F = 100 * \left(\frac{b}{c} - 1\right)$$

$$L = 100 * \left(\frac{a}{b} - 1\right)$$

where *F* is the planar anisotropy, *L* the linear anisotropy, *a*, *b* and *c* respectively the taller, medium and smaller axes of the ellipsoid. A positive Jelinek parameter will indicate an oblate ellipsoid, and a negative will indicate a prolate one.

2.2 Results

The results for samples NI13-01, NI13-02 and KA13-14 are indicated in the Table 1.

Table 1: results from 3D-ellipsoid approximation after least squares method on the dataset for samples NI13-01, NI13-02 and KA13-14. Shape is interpreted according to Jelinek parameter.

	NI13-01		NI13-02		KA13-14	
	Conductivity	P-wave speed	Conductivity	P-wave speed	Conductivity	P-wave speed
P%	10.8 %	8.5 %	5.6 %	6.4 %	6.7 %	15.9 %
T	0.894	0.016	-0.852	0.265	-0.310	0.121
Shape	oblate	triaxial	prolate	oblate	prolate	oblate

We can see in Table 1 that values of anisotropy percentage are weak. These anisotropies (around 10%) are not negligible, but not so much important in those lava samples. Nonetheless, Jelinek parameters present an important variation from a sample to another. NI13-01 has an important Jelinek parameter in thermal conductivity ellipsoid, but a quasi-triaxial parameter in P-wave propagation speed ellipsoid. NI13-02 has a prolate thermal conductivity ellipsoid, and an oblate P-wave ellipsoid, as KA13-14 sample. As NI13-02 presents the biggest Jelinek parameters, we will examine the 3D-ellipsoids (cf. Figure 3).

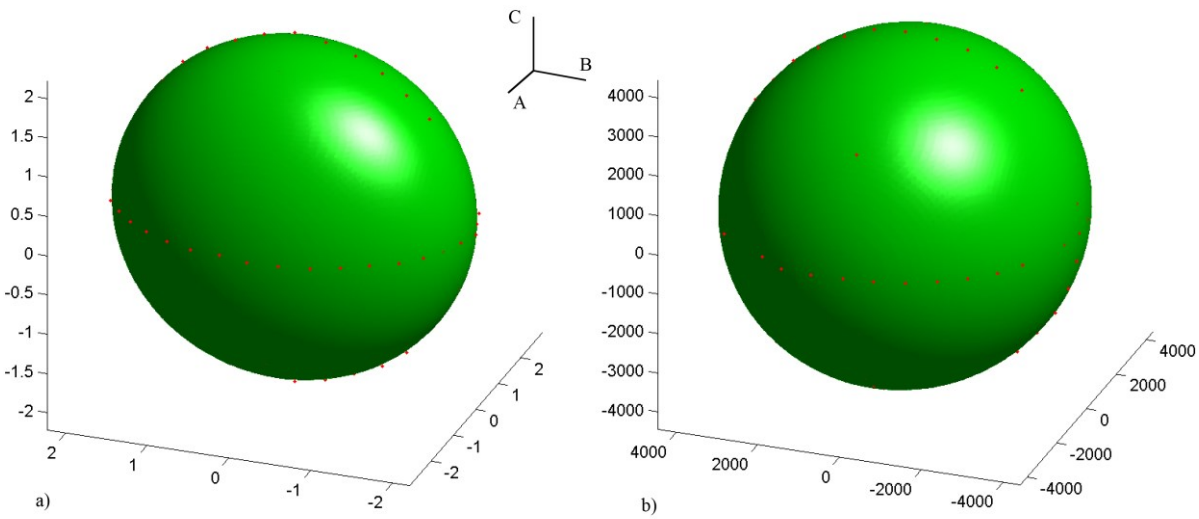

Figure 3: 3D-ellipsoids for sample NI13-02. a) represents thermal conductivity dataset, and b) represents P-wave propagation speed dataset. Thermal conductivities are expressed in $W.m^{-1}.K^{-1}$ and propagation speeds in $m.s^{-1}$. A, B and C are the three plug axes directions.

With the two ellipsoids we can observe that prolate axe of thermal conductivity seems to be collinear with axe of the plug B, although P-wave propagation ellipsoid oblate plane is perpendicular to this axe. If we observe the plug photographs (cf. Figure 4), we can mention the apparent alignment of minerals along the plan (A,C), in other words, the orthogonal plan to B. We can notice the seeming relation between macroscopic mineralogical anisotropies and petrophysical anisotropy directions.

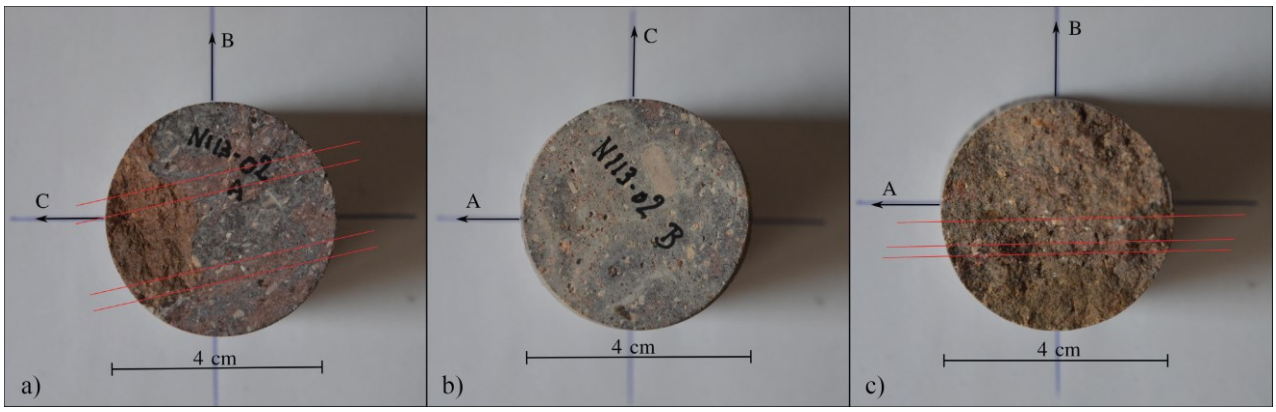

Figure 4: Plugs in three directions from sample NI13-02, with preferential apparent mineral directions highlighted.

In order to confirm or infirm the relation between macroscopic and petrophysical anisotropies, we examine the last volcano-sedimentary sample KA13-10. This one presents a clear macroscopic anisotropy, due to deposit layers and fractures along those layering directions.

The sample KA13-10 is more anisotropic than others. Moreover, the permeability was sufficient to permit us to measure it in three directions. Measures have been realized in three orthogonal directions, but we didn't make plugs, because of the evidence of macroscopic anisotropy. Results in Table 2 show us that petrophysical anisotropies are similar to macroscopic anisotropies. Direction C is orthogonal to the apparent layering, and directions A and B are coplanar to it. We can observe that directions A and B are in the same range of values, instead of direction C, which seems to highlight the macroscopic anisotropy.

Table 2: Average values of petrophysical measurements for sample KA13-10. Direction C is orthogonal to the apparent layering.

	Direction A	**Direction B**	**Direction C**
P-wave speed ($m.s^{-1}$)	2043	2343	899
Conductivity ($W.m^{-1}.K^{-1}$)	1.237	1.228	1.401
Permeability (mD)	47.5	13.4	3.5

2.3 Discussion

The first observation we can establish is the relation between macroscopic apparent anisotropy and petrophysical anisotropies. Thus, in sample KA13-10, the evident anisotropy is highlighted by the petrophysical results: P-wave propagation speeds are equivalent in directions A and B, and more important than in direction C. For the thermal conductivity, the contrast is weaker but shown. The question of the contrast in permeability values is harder to define, but in the detail, values of C direction permeability didn't exceed 5mD, although in directions A and B, the permeability range is far larger. This large range of permeability is due to the presence of micro-fracturing (which provoke an increase of permeability) and local mineralization (which decrease values) in direction of layering.

In the case of samples NI13-01, NI13-02 and KA13-14, anisotropies are less evident. Sample NI13-01 is apparently almost isotropic, with a triaxial ellipsoid for P-wave propagation speeds. The thermal conductivity ellipsoid shows an oblate anisotropy, but it can't be linked to a macroscopic anisotropy. Sample KA13-14 shows a weak anisotropy for both P-wave propagation speeds and thermal conductivities, but precipitation nodules seen in plugs can provoke those anisotropies. The case of sample NI13-02 is more interesting, because we can see a P-wave propagation speed oblate anisotropy, and a prolate one for thermal conductivity. The prolate direction axe is orthogonal to the oblate plane. So we have on the same axe a preferential conductivity direction, and a non-preferential P-wave propagation direction. That direction is oriented about axe B. As we can see in Figure 4, we can highlight with those anisotropies a preferential mineral plane (A-C plane), which is hard to see without petrophysical information.

Petrophysics and expression in a 3D-ellipsoid of anisotropy permit us to find some non-obvious planes or directions. In the case of the sample KA13-10, the anisotropic direction provokes a decrease of P-wave propagation speed, thermal conductivity, and permeability. That plane can be due to deposit layering and post-deposit fracturing in direction of deposit (decrease of both P-wave propagation and thermal conductivity). In the case of sample NI13-02, the measurement in 3D of petrophysical properties permits us to highlight a different kind of anisotropy: the decrease of P-wave propagation speed, and the increase of thermal conductivity. Those anisotropies are caused by a preferential direction of mineralisation in the flow and not to the fracturing.

Those petrophysical anisotropies are important to define the internal structuration of a reservoir block. As we can see, properties could present an important difference depending on the studied direction. Some of those properties are primarily important in a groundwater reservoir: permeability permits water circulation and thermal conductivity permits heat flow circulation, with or without convection.

3. MODELLING

The integration in numerical modelling of petrophysical anisotropies could give us more precisions in sustainability predicting for groundwater reservoirs. That information, used in complement to structural and regional information, will give us a good idea of the comportment of water and heat flows. We created a simplistic model in order to observe the influence of each anisotropy properties.

3.1 Tough2 Software and Graphical Output

The software used to simulate water flowing is Tough2, developed by the Berkeley University. This simulation software is based on separated equation-of-state modules. The equation-of-state module used, EOS1, is based on a one-phase simulation controlling temperature and pressure through time. This is the basic geothermal module, which permits space discretization, rocks properties definition water flow injection and production. That simple module gives us the possibility to test many different hypotheses.

The graphical output is realised with a Matlab homemade routine. We will study temperature repartition in the reservoir and water flow in different parts of it. The routine creates a regular mesh and interpolates values from Tough2 direct output files, and values are finally smoothed before displaying in two dimensions.

3.2 Model and Mesh Grid

The aim of this modelling is to compare, in most realistic situation, the influence of variations of petrophysical properties due to anisotropies on water and heat flow. In order to compare those different models, the grid had to be at same time realistic (in proportions, pressure and temperature conditions, etc.) and simplistic to permit to see differences between simulations.

Previous high scale models in Lesser Antilles, e.g. Lachassagne et al. (2009), Bouchot et al. (2010) or Lopez et al. (2010) in Guadeloupe, did not permit to work on reservoir partitioning. Later, Calcagno et al. (2012) realized a 3D structural modelling which highlighted relation between faults and offered us the opportunity to better understand geometry of the reservoir. Based on literature, e.g. Eurafrep (1970) for BO.3 borehole in Bouillante geothermal field, we defined a block, separated by two vertical faults (cf. Figure 5). The block is vertically separated in two main parts: the superior part represents a lava flow, and the inferior is volcano-sedimentary deposit. Authors described later this template, e.g. Mas et al. (2006) in BO.5 and BO.6 borehole descriptions and analysis. Each cell measure one meter per one, and is extruded on two meters. We will work vertically, in two dimensions to simplify simulation.

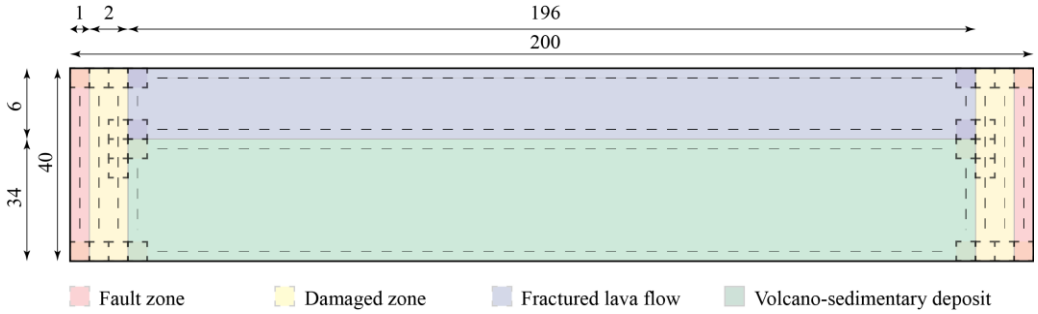

Figure 5: Mesh grid created to model a reservoir block. Lengths are in meters.

3.3 Limit Conditions and Property Values

Simulation was run in most realistic limit conditions temperature to be close to real pressure-temperature conditions in Bouillante geothermal field. Temperatures gave in production depths between 500 and 900 meters are about 240-270°C, and pressure about 90-100 bar, e.g. Eurafrep (1970), Brombach et al. (2000), Sanjuan et al. (2001), Guillou-Frottier (2003), Mas et al. (2006), Lachassagne et al. (2009). We chose to use maximal values for pressure and temperature respectively. Production in the block is made at the top of the right fault, and refill simulated is natural refill, at the base of both faults, approximately at reservoir temperature.

Property values for the different parts of the block were taken from different works, e.g. Violay (2010) and Bernard et al. (2007). Fractured lava flow permeability is an average from basalts permeability values taken from Violay (2010), although thermal conductivities are measured values on Kayserstuhl sample KA13-14. Both volcano-sedimentary deposit permeability values and thermal conductivity values are taken from laboratory measurements on Kayserstuhl sample KA13-10. In the fault zone and damaged zone, we used proper fault zone values for porosity and permeability, and lava flow thermal conductivities.

In order to test influence of anisotropies, we will sit our observations on an isotropic model (cf. Figure 6 for simulation results and Table 3 for values). Then we will observe two different possibilities: one to test permeability anisotropy, using different values in horizontal and vertical directions, based on laboratory measurements, the other to test the influence of thermal conductivity contrasts. Thus, Haffen et al. (in prep) proved the influence of porosity on thermal conductivity, using thermal conductivity mapping on granite and sandstone samples. After simulation, they observed an influence of thermal conductivity repartition on water circulation. We will integrate this work decreasing thermal conductivity values in fault and damaged zones, to see influence on water flow simulation. A third hypothesis is modelled, in the case of an injection well refill the block at the base of right fault. Temperature taken for this injection well is temperature after geothermal treatment in Bouillante: about 60°C. This simulation aims to highlight the sustainability of the system with a hypothetic injection well, and the influence of petrophysical anisotropies on the system.

Table 3: Petrophysical property values used to simulate the reference model.

	Volumetric mass ($kg.m^{-3}$)	Porosity	Permeability (m^2)	Thermal conductivity ($W.m^{-1}.K^{-1}$)
Fault zone	2700	0.50	$2 \cdot 10^{-10}$	2.1
Damaged zone	2700	0.19	$1 \cdot 10^{-12}$	2.1
Fractured lava flow	2870	0.03	$1 \cdot 10^{-14}$	2.1
Volcano-sedimentary deposit	2650	0.15	$5 \cdot 10^{-14}$	1.4

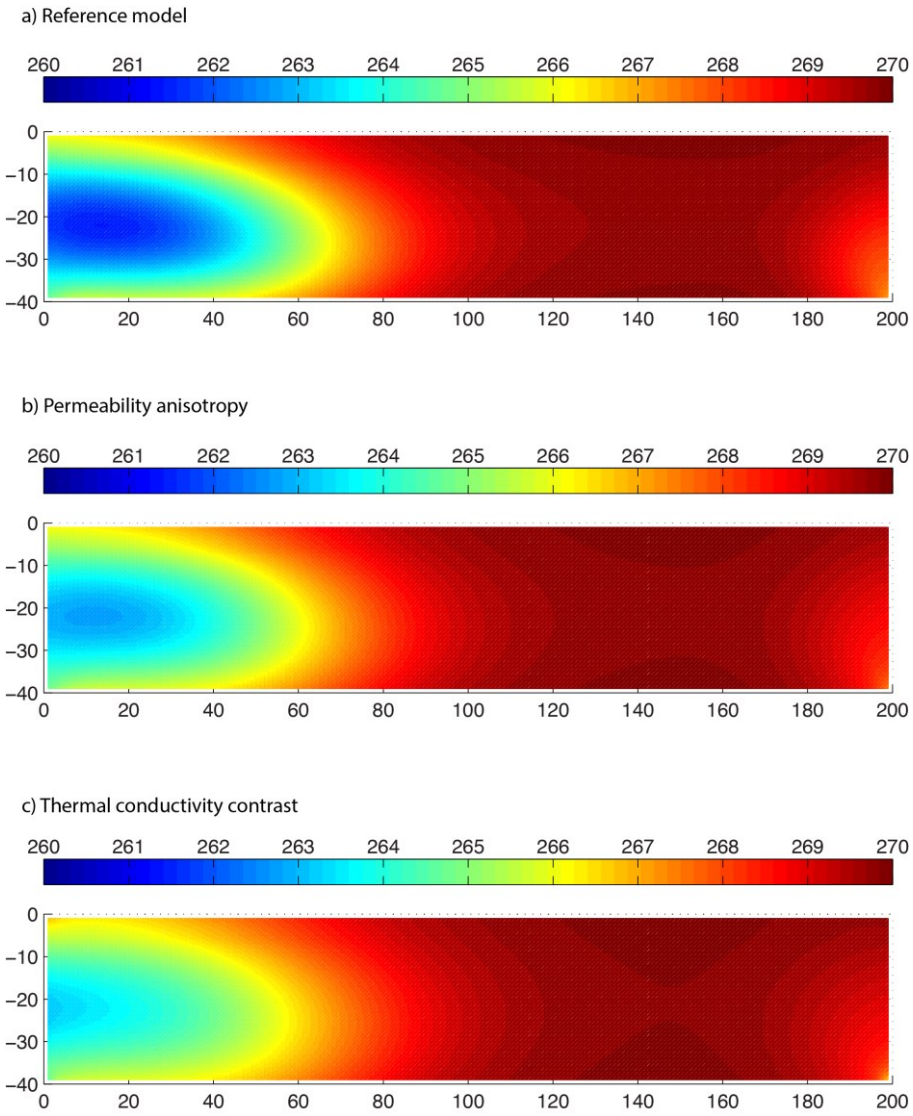

Figure 6: Temperature maps after 20 years simulation. Production well is at the top of the right fault, refill is made at the base of both faults. a) is reference model, b) is permeability anisotropic model and c) is model using thermal conductivity contrast. x and y axes are in meters, temperatures are in °C.

3.4 Results

Figure 6 shows resulted temperatures after twenty years simulation. We can observe the different cases, and implication on temperatures repartition: a) is the reference simulation, petrophysically isotropic, b) is the result of simulation with permeability anisotropies integrated, and c) is the result of simulation with conductivity contrasts. We can observe clear differences between these simulation results, but in order to highlight the influence on the flowing rate in the block, we realized graphical output for flow rate repartition. Figure 7 shows resulted flow rates for the same simulation time. Cases a), b) and c) are the same as in Figure 6, and lines in the left part of each figures are graphical output artefacts.

Based on Figures 6 and 7, we can see some apparent differences. From comparison between 6a and 6b, we can see that permeability anisotropy influence the vertical propagation of the heat flow. In case 6b, the cold bulge seems to be thinner than in

reference case 6a. This hypothesis is highly confirmed by the flow rates comparison (between 7a and 7b): 7b's flow rates are more spread and less important than flow rates in isotropic case 7a. Moreover, when in Figure 7a we can see the creation of sort of convection cells. The creation of those cells is not observed with permeability anisotropy. From comparison to 6a and 6c, we can see that horizontal propagation of heat flow is slowed by the weaker conductivity of the main circulation zones: fault and damaged zones. Observing flow rates, convective cells are well marked in 7a, but less in 7c, with the top cell even open at it left side, in contact with the damaged zone.

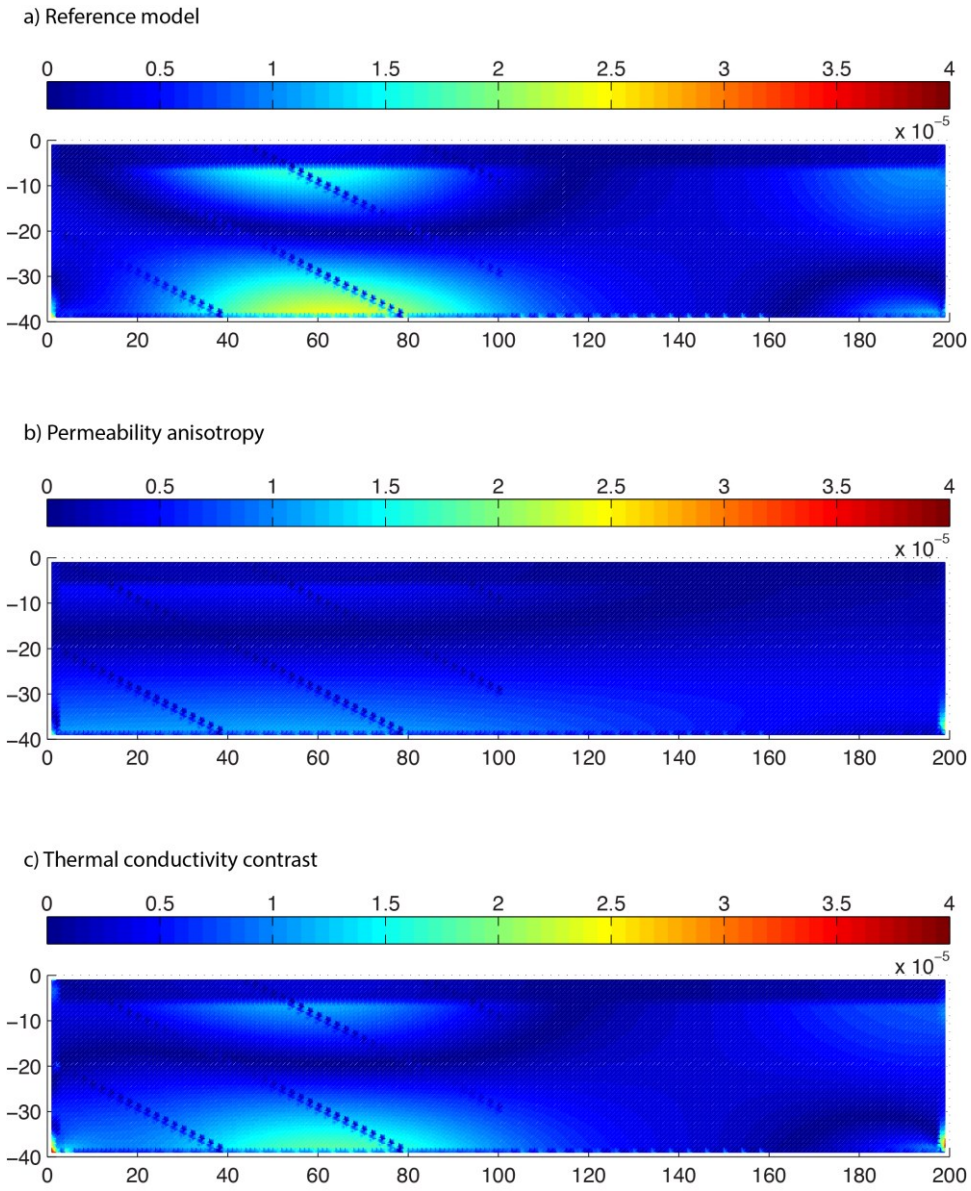

Figure 7: Fluid flow rates maps after 20 years simulation. Production well is at the top of the right fault, refill is made at the base of both faults. a) is reference model, b) is permeability anisotropic model and c) is model using thermal conductivity contrast. x and y axes are in meters, flow rates are in kg.s^{-1}.10^{-5}.

In order to confirm our observations, we realised three more simulations re-injecting water at the base of the right fault. Figure 8 shows influence of the two parameters on flow rates. In case of permeability anisotropy (cf. Figure 8b), the result is the non-creation of convection cells and the concentration of horizontal flows, only in the right part of the block. On Figure 8c, with a thermal conductivity contrast between circulation zones, we can observe the reduction of horizontal flowing outside of the fault zone. Moreover, the shape of the convection cells is quite different, and new cells even appear in the left fault zone.

3.5 Discussion

Observing these results between them permits us to extract some information. First, we observed the creation of sort of convection cells in almost every model. These convection cells are more or less intense and large, depending on the petrophysical parameters and injection properties. The common point of every convection cell is the localisation: cells seem to be initiated by a property contrast as at the bottom of the block, or at the limit between volcano-sedimentary deposit and fractured lava flow. The convection is an evidence of both vertical and horizontal flows in the volcano-sedimentary matrix. Circulations inside the matrix are regulated by permeability properties, as we can see in anisotropic example, which provoke the non-initiation of convection cells.

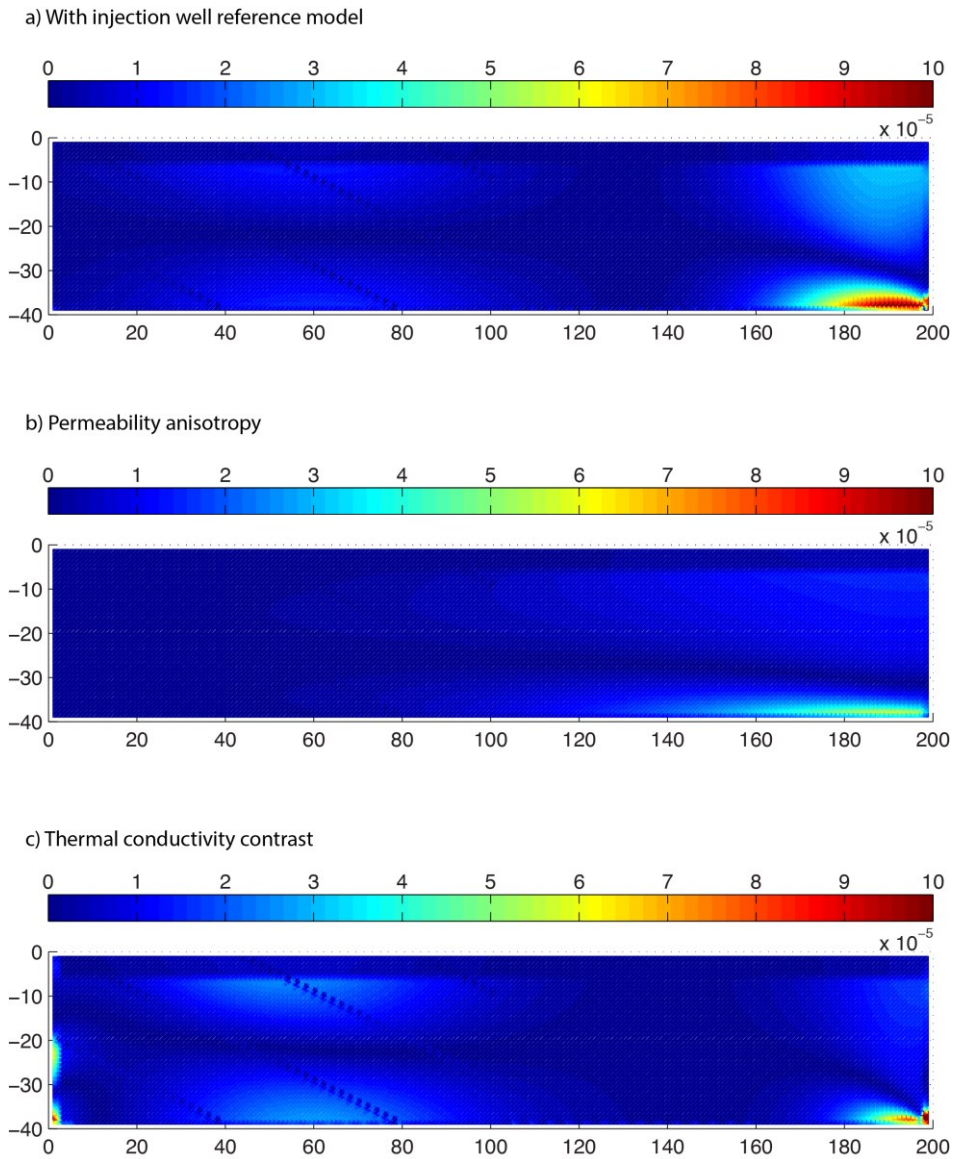

Figure 8: Fluid flow rates maps after 20 years simulation. In those models a injection well is simulated at the base of the right fault, the production well is at the top of the right fault. a) is reference model, b) is permeability anisotropic model and c) is model using thermal conductivity contrast. x and y axes are in meters, flow rates are in $kg.s^{-1}.10^{-5}$.

Then, we can see obvious differences of flow rates depending on the permeability anisotropies, but simulations highlight the influence of thermal conductivity in flow rates geometry as well. In fact, we can see the influence of both parameters on heat flow and fluid flow. The thermal conductivity contrast between circulation zone and volcano-sedimentary deposit seems to create a channelization of water flow, like if the simple presence of a thermal conductivity contrast was equivalent to a permeability contrast.

Finally, in both natural refill of the block and injection well refill, we can observe horizontal flows. Those circulations, inside the matrix, provide the evidence of the non-exclusive flow in the faults. Matrix flow permits heat and fluid circulations, which are influent on the reservoir temperature, and so is on the reservoir sustainability.

4. DISCUSSION

Determination of petrophysical anisotropies permits us to test different model hypothesis and measure the influence of each parameter on the simulation. First parameter is permeability, which has an obvious impact on flow rates and water circulation geometry. The isotropic permeability permits the creation of convection cells, as permeability anisotropies stop this phenomenon. The second parameter to play a role is the presence of thermal conductivity contrasts, which modifies the heat flow and the heating of the water circulating in the reservoir. A bad thermal conductivity will increase the influence of convection effect and convection heat flow (thanks to the convection fluid flow), although a good thermal conductivity will permit heat diffusion by conduction and the heating of the cold water (in the case of the presence of an injection well). This will have a great influence on the reservoir time life.

Moreover, we saw thermal conductivity contrasts had an influence on fluid flow rates too. A high thermal conductivity contrast provokes the channelization of the circulations, as a physical barrier. This effect is really important to understand groundwater

circulation, because we could establish a direct link between thermal conductivity contrasts and apparent permeability. In our modelling, we could not simulate thermal conductivity anisotropies in the three space directions, but it could be interesting to draw a link between thermal conductivity and apparent permeability mapping, in order to artificially model thermal conductivity anisotropies.

Those anisotropies are now better understood in modelling, but we can discuss their origin. In the case of volcano-sedimentary deposit, it probably highlights the deposit plans, or in the case of ash flow, the flow direction. In the case of lava flows, it can be the flowing direction mark. It can also be an evidence of structural anisotropies, caused by post-depositional deformation. Using those anisotropies can give us tools to better understand deformations and even help to identify structural heritage.

5. CONCLUSION

As we saw with the petrophysics part, rocks can present more or less anisotropies. Those anisotropies could be underlined by macroscopic apparent anisotropies, but some of rock samples appear to be macroscopically isotropic. Petrophysical methods permit us to highlight anisotropies, which can be the witness of a flow direction during deposition, a post-formation deformation, or the structural heritage. Those small anisotropies, at reservoir scale and exploitation time, can change the comportment of water flow inside the reservoir, and have an influence on the heat and fluid circulations.

Moreover, simulation underlines the importance of the precise definition of petrophysical anisotropies (permeability and thermal conductivity) in order to better constrain and understand geothermal reservoirs. Models allow us to see and evaluate horizontal transfers in those reservoirs: the circulation is not restrained to the fault itself, but circulation inside the fault zone provokes horizontal transfers in the matrix around. Those transfers play a capital role in water heating in a case where injection well is used to evacuate geothermal water after energy extraction.

REFERENCES

Bernard, M.-L., Zamora, M., Géraud, Y., and Boudon, G.: Transport Properties of Pyroclastic Rocks from Montagne Pelee Volcano (Martinique, Lesser Antilles)., *Journal of Geophysical Research-Solid Earth*, 112, no. B5, (2007).

Birch, F.: The Velocity of Compressional Waves in Rocks to 10 Kilobars, Part 1., *Journal of Geophysical Research*, 65, no. 4, (1960), 1083–1102.

Bouchot, V., Traineau, H., Guillou-Frottier, L., Thinon, I., Baltassat, J.-M., Fabriol, H., Bourgeois, B., and Lasne, E.: Assessment of the Bouillante Geothermal Field (Guadeloupe, French West Indies): Toward a Conceptual Model of the High Temperature Geothermal System., *Proceedings World Geothermal Congress 2010*, edited by International Geothermal Association, 8 p., Bali, Indonésie, (2010).

Bourdon, E., Bouchot, V., Gadalia, A., and Sanjuan B.: Geology and Geothermal Activity of the Bouillante Volcanic Chain., BRGM, (2011).

Brombach, T., Marini, L., and Hunziker, J., C.: Geochemistry of the Thermal Springs and Fumaroles of Basse-Terre Island, Guadeloupe, Lesser Antilles., *Bulletin of Volcanology*, 61, no. 7, (2000).

Calcagno, P., Bouchot, V., Thinon, I., and Bourgine, B.: A New 3D Fault Model of the Bouillante Geothermal Province Combining Onshore and Offshore Structural Knowledge (French West Indies)., *Tectonophysics*, 526–29, (2012), 185–95.

Eurafrep. Coupe Géologique Interprétée Du Forage BO.3, Bouillante, Guadeloupe., *Fiche dossier du sous-sol - Relevé de forage*, BRGM, (1970).

Guillou-Frottier, L. Compilation et Analyse Des Données Thermiques Sur Le Champ Géothermique de Bouillante. Premières Interprétations Pour Le Fonctionnement Du Champ Géothermique., *Rapport Final*, BRGM, (2003).

Haffen, S., Bur, N., Perry, G., Rosener, M., Géraud, Y., and Diraison, M.: Rock-Fluid Heat Exchanges, Input from Thermal Conductivity and Porosity Mapping for Different Rock Structures., (in prep).

Lachassagne, P., Marechal, J. C., and Sanjuan, B.: Hydrogeological Model of a High-Energy Geothermal Field (Bouillante Area, Guadeloupe, French West Indies)., *Hydrogeology Journal*, 17, no. 7, (2009), 1589–1606.

Lopez, S., Bouchot, V., Lakhssassi, M., Calcagno, P., and Grappe B.: Modeling of Bouillante Geothermal Field (Guadeloupe, French Lesser Antilles)., *Proceedings*, 35th Workshop on Geothermal Reservoir Engineering, Stanford University, Stanford, California, SGP-TR-1988, (2010).

Mas, A., Guisseau, D., Patrier Mas, P., Beaufort, D., Genter, A., Sanjuan, B., and Girard, J.-P.: Clay Minerals Related to the Hydrothermal Activity of the Bouillante Geothermal Field (Guadeloupe)., *Journal of Volcanology and Geothermal Research*, 158, no. 3–4, (2006), 380–400.

Nédélec, A., and Bouchez, J.-L.: Pétrologie Des Granites, *Société Géologique de France*, Éditions Vuibert, (2011).

Popov, Y., A., Dan, F., C., Pribnow, J., H., Sass, C., Williams, F., and Burkhardt, H.: Characterization of Rock Thermal Conductivity by High-Resolution Optical Scanning., *Geothermics*, 28, no. 2 (1999), 253–76.

Sanjuan, B., Brach, M., and Lasne E.: Bouillante Geothermal Fluid: Mixing and Water/rock Interaction Processes at 250 °C., 10–15, Cagliari, Italy, (2001).

Violay, M. Réservoirs Hydro-Géothermaux Haute Enthalpie : Apport Des Propriétés Pétrophysiques Des Basaltes., Montpellier 2, (2010).